Research Article | Vol. 30, No. 9 / 25 Apr 2022 / Optics Express 15566
Optics EXPRESS

X-ray Fourier transform holography with beam shaping optical elements

C. Pratsch,[1,*] S. Rehbein,[1] S. Werner,[1] P. Guttmann,[1] H. Stiel,[2] and G. Schneider[1,3]

[1]Helmholtz-Zentrum Berlin für Materialien und Energie, Dep. X-Ray Microscopy, Albert-Einstein-Str. 15, 12489 Berlin, Germany
[2]Max-Born-Institut für Nichtlineare Optik und Kurzzeitspektroskopie im Forschungsverbund Berlin e.V., Max-Born-Straße 2 A, 12489 Berlin, Germany
[3]Humboldt-Universität zu Berlin, Mathematisch-Naturwissenschaftliche Fakultät, Institut für Physik, Newtonstraße 15, 12489 Berlin, Germany
*christoph.pratsch@helmholtz-berlin.de

Abstract: Holography is a powerful method for achieving 3D images of objects. Extending this method to short wavelengths potentially offers significantly higher resolution than visible light holography. However, current X-ray holography setups employ nanoscale pinholes to form the reference wave. This approach is relatively inefficient and limited to very small sample size. Here, we propose a new setup for X-ray holography based on a binary diffractive optical element (DOE), which forms at the same time the object illumination and the reference wave. This optic is located separately from the sample plane, which permits investigation of larger sample areas. Using an extended test sample, we demonstrate a resolution of 90 nm (half-pitch) at an undulator beamline at BESSY II. The new holography setup can be directly transferred to free electron laser sources enabling time-resolved nanoscale imaging for ultra-fast processes.

1. Introduction

Soft X-ray imaging is routinely used in biomedical and materials science research. Well established applications include soft X-ray absorption spectromicroscopy and nanoscale X-ray tomography. Due to their short wavelength and relatively strong interaction with matter, soft X-rays are well suited to investigate processes and materials with a spatial resolution of a few nanometers. To study fast dynamic processes on the nanometer scale, the existing synchrotron based X-ray imaging methods cannot be easily transferred to X-ray free electron lasers (FEL) with their high brilliance [1]. Due to the high photon flux in single shots, X-ray imaging at an FEL source causes typically high heat load to the sample. Therefore, the FEL provides basically only single shot imaging. Furthermore, imaging at the FEL requires coherent imaging methods due to the high degree of coherence [2–4]. X-ray holography fulfills these criteria and is ideally suited for single shot imaging of extended samples at FELs.

Holography is well established for visible light [5] and for nanoscale imaging in electron microscopy [6]. Both methods have in common that very efficient optics exist. In contrast, X-ray is lacking efficient high NA optics. Therefore, most X-ray holography setups do not contain X-ray optics. Instead, one or several nanoscale transparent pinhole(s) in an opaque screen generate the reference wave(s) and a larger pinhole restrict the illumination of the sample area. The diffracted waves from the sample area and the nanoscale pinhole(s) interfere to form the hologram on the detector [7]. All pinholes have to be coherently illuminated to form an interference pattern which encodes the structural information about the sample. Under these conditions, the image of the object is recovered by a simple Fourier transform of the hologram in the far-field.

These lensless holography setups have some drawbacks. Due to the small nanoscale pinhole size only an extremely small part of the incident photon flux is used to form the reference wave.

#453747 https://doi.org/10.1364/OE.453747
Journal © 2022 Received 2 Feb 2022; revised 27 Mar 2022; accepted 3 Apr 2022; published 21 Apr 2022

Optics EXPRESS

In addition, pinholes and sample have to be mounted roughly in the same plane. In practice, this causes severe limitations on the sample environment and prevents the investigation of relevant biomedical and material science specimens [8–12]. Hence, X-ray holography is relatively rarely used for X-ray imaging. Instead zone-plate based X-ray microscopy and ptychography dominate the field.

With the growing number of FELs and the upcoming fourth generation electron storage rings with their high degree of coherence, X-ray imaging would benefit from the development of an efficient holography setup, which overcomes the limitations on the sample environment. This motivated us to develop a new setup for X-ray holography, which enables application of X-ray holography for extended samples without the need to couple sample and optical elements as in current setups. Our approach is based on a new diffractive optical element (DOE), which is located in front of the sample plane and, therefore, frees the space in the sample plane for manipulating larger objects. The DOE pattern is designed in such a way that it simlutaneously provides both the required reference wave and the sample illumination. The intensity distribution generated in the plane of the sample consists of two spots, a small bright reference spot and a significantly larger and dimmer spot for the illumination of the sample (see also Fig. 2 a). We find that the signal-to-noise ratio for imaging is optimized when the number of photons in the reference wave is in a range comparable to the number of photons diffracted by the sample. The DOE pattern can be tuned to achieve this optimum.

2. Experimental setup

A serious problem for X-ray based inline holography is the so-called twin image problem. We can solve this problem by laterally separating the reference wave from the wave illuminating the sample. In previous setups this lateral separation has been realized by two pinholes, one larger pinhole for the sample and a nanoscale pinhole for forming the reference wave (Fig. 1 a). Instead of illuminating these pinholes by a coherent wave, we replace the pinholes in our new design with a binary diffractive optical element (DOE) in front of the sample plane which simultaneously produces the reference wave and the illumination of the sample. With this holography setup (Fig. 1 b), we fulfill the conditions for Fourier transform holography (FTH). Therefore, the image can be derived from a simple Fourier transform of the hologram.

In order to optimize the image quality with maximum contrast and spatial resolution, different constraints must be addressed: a) the reference spot determining the lateral resolution has to be small, b) for optimal contrast of the hologram the photon flux passing through the reference and sample have to be matched and c) the lateral separation between the sample and reference has to be large enough to avoid an overlap of the image and the central peak in the Fourier transform. These considerations were incorporated into an in-house developed algorithm [13] that we used to compute the DOE. From a mathematical point of view, the algorithm is essentially a fixed-point iteration on a non-convex set (see figure S 5). Due to the size of the DOE, the algorithm was split into two components: a Fresnel diffraction and phase unwrapping based fast iterator and a final finer interpolator. For the Fresnel diffraction component we assumed that the DOE acts purely on the phase of the incoming wave. Therefore, the target intensity distribution might not be within the set of possible solutions, which causes in our case a double peak (see Fig. 2 b and c). However, the efficiency of the optic increases in comparison to an intensity modifying one, since less photons are absorbed. This algorithm is available upon reasonable request. Recently, an alternative algorithm has been proposed [14]. This algorithm was used in [15] for a purely numerical simulation to realize a similar approach to ours [13,16]. However, the results in [15] suggest that this algorithm is problematic for optics with relatively large central stop, such as the one required for our experiment.

The DOE used in our experiment had a diameter of 400 μm, a central stop of 200 μm and a focal length of 5.2 mm at a wavelength of $\lambda = 3.84$ nm. Its outermost average structure size is

Optics EXPRESS

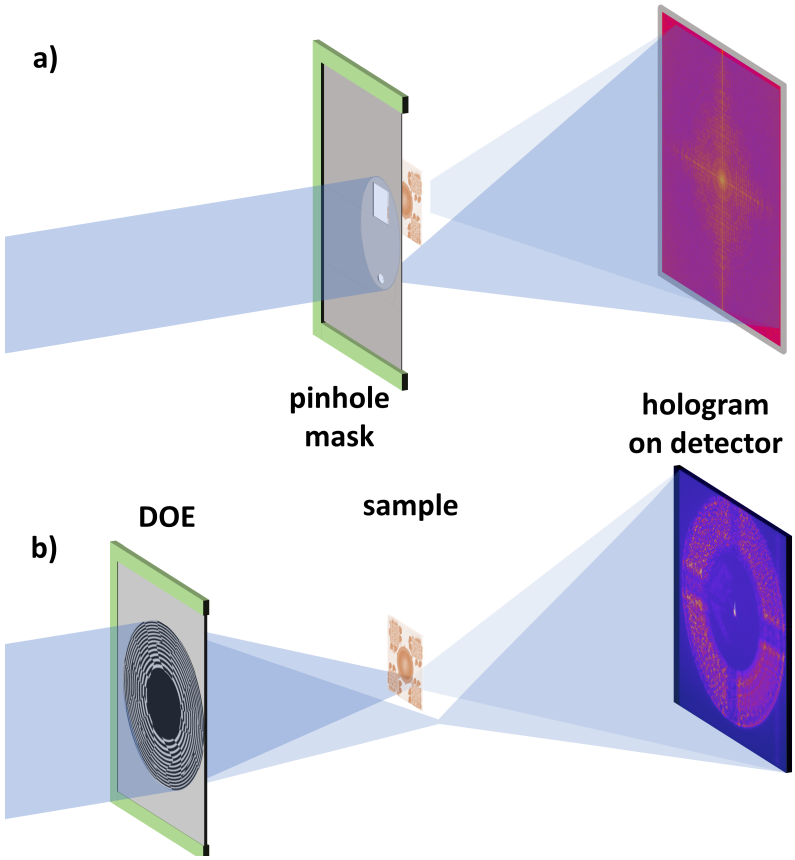

Fig. 1. Comparison between the pinhole and DOE based approach to holography. a) A set of pinholes defines the illumination of the sample and the reference wave. b) The DOE forms the reference and the sample illumination. In both cases the optics are illuminated by an incident quasi monochromatic coherent wave field. The hologram results from the interference between reference and sample wave. The hologram is detected on a pixelated detector

about 50 nm. The spot for the sample illumination had a square shape with length of 5 µm. The distance between reference spot and sample spot was 10 µm. In Fig. 2 a, the intensity distribution generated by the DOE is shown.

As test sample, we used 120 nm high gold structures on a Si_3N_4 membrane. The sample consisted of four square areas which included a pattern of "T"-shaped structures in various orientations (see Fig. 3 b and d). Each area also included four Siemens star patterns which had spikes between 20 nm and 100 nm width. In the center of the sample, we placed a high resolution Fresnel zone plate (FZP) with 201 zones and an outermost zone width of 39.1 nm. This zone plate was also used for alignment purposes and to image the focal pattern of the DOE. The DOE and a test sample were fabricated using an electron beam based lithography process at the Helmholtz Zentrum Berlin.

The X-ray holography experiment was conducted at the U41-SGM-TXM beamline at BESSY II [17] using the existing transmission X-ray microscope (TXM) end-station. Due to the limited space around the sample area in the TXM, we did not include a separate pinhole for the order sorting aperture (OSA). Instead, a central stop was added to the window of the DOE wafer (see

Optics EXPRESS

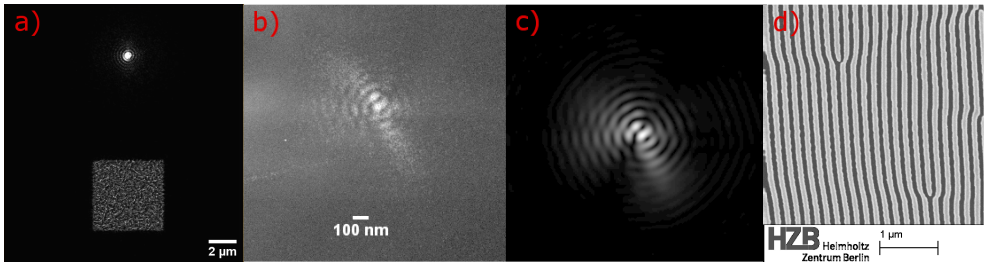

Fig. 2. a) Numerically simulated intensity profile in the focal plane of the DOE. The bright spot is used as reference and the square area illuminates the sample. b) and c) Comparison between the measured reference spot produced by the DOE (b) and the simulation of the spot (c) by numerical solution of the Rayleigh-Sommerfeld diffraction integral via Green functions. Both images are scaled for the same resolution. The DOE is designed to only shift the phase of the incident wave. This has the advantage of a higher diffraction efficiency but leads to constraints on the possible intensity distribution in the focal plane of the DOE [18], one example being the substructure of the reference spot. d) SEM micrograph showing a small part of the DOE structure. The overall structure of the DOE is very similar to a Fresnel zone plate pattern, but also contains some branching points.

figure S2). The central stop was matched to a 100 µm x 100 µm-width thin Si_3N_4 membrane that carried the test sample, so that this window formed an order-sorting aperture.

As detector, we used the thinned, backside illuminated CCD of the TXM (Roper Scientific, PI SX1300). The distance between the focal plane of the DOE and the CCD was 320 mm, thus fulfilling the Fraunhofer far-field approximation which is required for the FTH approach. Under these conditions, the numerical aperture (NA) was $NA \approx 0.04$, which yield an Abbe diffraction limit of about 50 nm for a wavelength of $\lambda = 3.84$ nm. As a first step to evaluate this approach, we measured the light distribution generated by the DOE in the focal plane of the DOE. For this purpose, we used a high resolution Fresnel zone plate with $dr_N = 25nm$ to form an enlarged image of the intensity distribution on a CCD. Figure 2(b,c) shows a comparison between the numerically calculated and the measured focal spot, which are in good agreement.

In a second step, the previously described test sample containing also a FZP was inserted into the beam path. In order to calibrate the position of the test sample with respect to the DOE, the light distribution in the focal pattern of the DOE was imaged with this FZP. Afterwards, we shifted the sample by the known imaging length of the FZP, so that the sample was in the focal plane of the DOE. In order to image an extended sample area, we raster scanned an area containing the test structures. The scanned area was 40 µm × 46 µm at a step width of 2 µm. In order to normalize these images, flat field holograms should ideally also be recorded. Since in our case the thinned wafer window was also used as OSA, we could not remove the sample, which made it impossible to acquire flat-field images. Therefore, the underlying illumination profile had to be interpolated from the experimental data, which will be discussed in the method section.

Optics EXPRESS

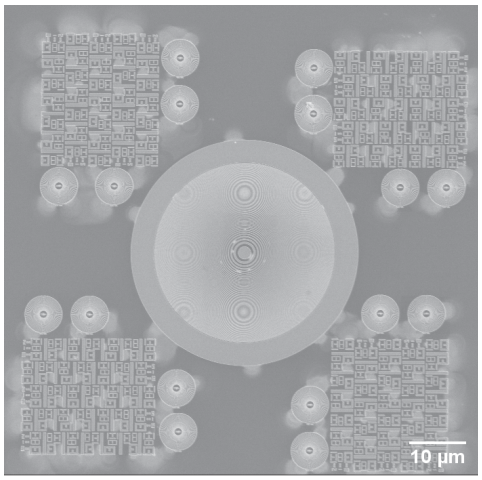

a) SEM overview of the test sample.

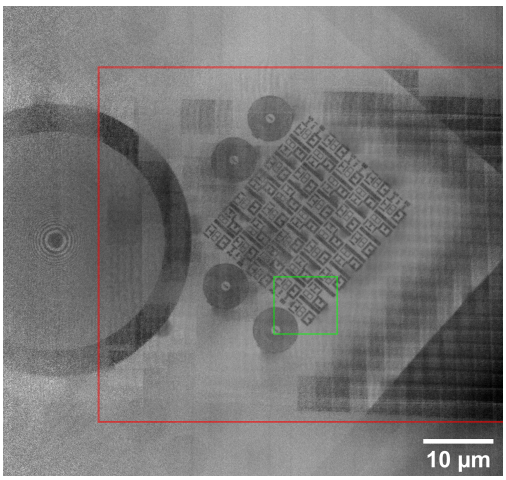

b) FTH based extended reconstruction.

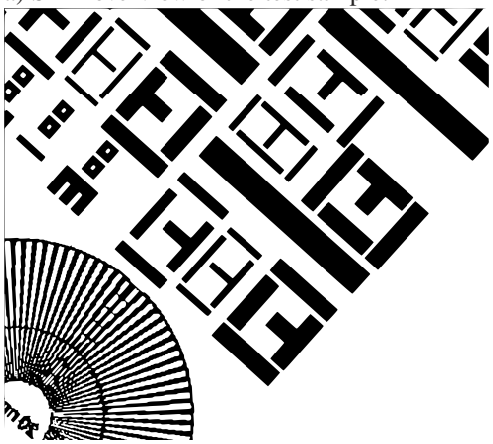

c) Design pattern of green frame in b).

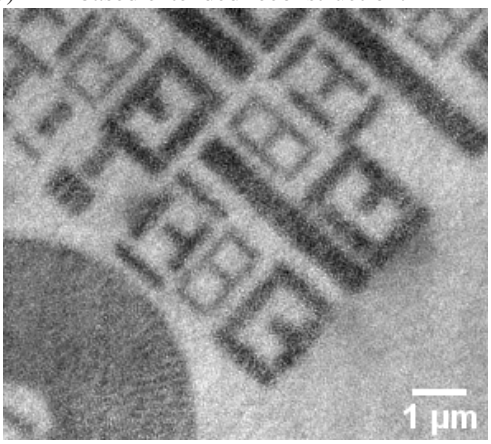

d) Zoom in on green frame of b).

Fig. 3. a) SEM image of the test sample. b) FTH reconstruction based on an extended scan (the red frame shows the area scanned by the object spot). A remarkable observation is, that the field of view extends far further than the area that was scanned by the bright square object spot. (see also Fig. 2, a) c) The design charts for the sample corresponding to the green frame in (b). d) Detailed view of the reconstruction shown in (b), showing a Siemens star pattern with a diameter of 6.5 µm and outermost spikes of 100 nm (not fully resolved). The structure width of the "T" is 100 nm, 200 nm and 300 nm respectively.

Optics EXPRESS

3. Method

The reconstruction of the sample based on the holograms requires the knowledge of additional parameters of the experiment, namely the wavelength, the position of the sample at each exposure, the distances between the DOE, sample and CCD. The wavelength is defined by the monochromator settings and recorded during the experiment. The distance between the DOE and CCD was recovered from the known focal length of the DOE, the wavelength used and the experimental holograms.

In order to reconstruct an image of the extended sample, holographic reconstructions at the different scanning positions have to be merged. However, this merging step requires that the individual holograms are normalized beforehand to take into account the effects of the object illumination.

Therefore, similar to classical microscopy, we correct the illumination effect with flat-field images. However, as noted above, our setup does not permit shifting the object completely out of the optical path, since it is also used as part of the OSA. Therefore, the flat-field had to be estimated. Due to the knowledge about our test sample, we were able to choose a sub-series of images that contained almost no strongly absorbing structures. A first estimate of the flat-field is the mean of this image series. However, the mean is strongly influenced by outliers. In contrast the median is known to be more robust against outliers. For this reason, the median was chosen as an estimator for the flat-field.

In the next step the resolution in the sample plane was determined. The distance between detector and focal plane relates the size and resolution of the detector to the size and number of pixels in the holographic reconstruction. The exact relationship depends on the numerical Fresnel propagator used. In our case the relationship was $\Delta_2 = \frac{\lambda z_{1,2}}{\Delta_1 N}$. Here, Δ_1 is the resolution in the first plane and Δ_2 is the resolution in the second plane, $z_{1,2}$ is the distance between first and second plane and N is the number of pixels along the considered dimension.

After determining all required parameters, the image of the sample can be recovered via Fourier transform holography (FTH) [16]. The theoretical background for the FTH approach is based on the Fraunhofer approximation. Under these conditions, the far-field hologram is proportional to the Fourier transform of the field in the sample plane. In a Fraunhofer FTH experiment, the intensity on the detector results from an interference between the reference and the scattered field

$$I_{detector} = \left|\psi_{reference} + \psi_{sample}\right|^2 .$$

Here, $\psi_{reference}$ and ψ_{sample} represent the propagated wave fields on the detector. In the FTH method, a Fourier transform leads to a reconstruction of the sample [5]

$$\begin{aligned}\mathcal{F}^{-1}\left[I\right] \propto\ & U_{ref} * \left(\overline{U_{ref}} \circ -Id\right) + \underline{U_{sam} * \left(\overline{U_{ref}} \circ -Id\right)} \\ & + \underline{U_{ref} * \left(\overline{U_{sam}} \circ -Id\right)} + U_{sam} * \left(\overline{U_{sam}} \circ -Id\right).\end{aligned} \tag{1}$$

Here, U_{sam} and U_{ref} are the field in the plane of the sample and reference. $\mathcal{F}^{-1}$ denotes the inverse Fourier transform operator, $-Id$ the point reflection at the origin, $\circ$ the composition and $*$ the convolution operator. The two underlined terms in Eq. (1) represent the FTH reconstructions of the sample. Since the result is a convolution between reference and sample wave field, these reconstructions are blurred by the shape of the reference. Therefore, a small and well-defined reference spot in the sample plane is essential. For an optimal signal-to-noise ratio of the reconstruction, the underlined terms should be large in comparison to the non-underlined terms. During the design of the DOE one can optimize the illumination accordingly.

In the following, we explain the reconstruction step required for recovering the extended test sample (see SEM image in Fig. 3 c). The reconstruction was done by merging together the FTH

Optics EXPRESS

reconstructions which were taken at different lateral sample positions. The merging process included a weighted averaging which reduces the deterioration of the resolution by speckles. One limitation of the quality and resolution of the resulting image was the precision of the positions used for stitching. Since the logged positions from the motor encoders had absolute errors on the order of several hundred nanometers, they were not sufficiently accurate for a high-resolution reconstruction. Hence, the logged positions were only used for a rough, first alignment and were sequentially improved by a semi-automatic alignment algorithm.

For this purpose, different alignment methods were tested. Due to the speckle noise in the single images, the supplied image-registration routines in Matlab [19] did not work reliably. Therefore, we aligned the single holographic reconstructions manually. The corrected positions were then used to generate an image of the test sample (see Fig. 3 b) and d)). The test sample image was generated in three steps. First, a mask was used to remove the central bright spot in the single frame holographic reconstruction (see Eq. (1) first and last term in the sum). Second, the extended reconstruction was built from these single frame reconstructions by alignment-dependent weighted averaging, which means that at a specific pixel the resulting reconstruction is the sum of all pixel values of the corresponding single frame holographic reconstructions. Third, the result was then normalized by the sum of the corresponding flat-fields. In this way, the reconstruction takes into account the effects introduced by the photon-statistics.

The spatial resolution is an important parameter for any imaging method. In order to evaluate the achieved resolution, we used the Fourier Ring Correlation (FRC) method [20]. In order to apply the FRC, the data set was split into two disjoint subsets. Each data set was then reconstructed and a sub-part of the two results used as the input of the biop.frc implementation in ImageJ [21]. Due to the scanning process, outer parts of the reconstructed image have been exposed to less photon numbers than the central part. Due to the lower signal-to-noise ratio, we expected the lateral resolution to decrease towards the border of the image. In fact, the measured FRC resolution for the central part shown in Fig. 3 d) was 92 nm (half-pitch), while at the border the center of the zone plate was still recovered with a resolution slightly better than 150 nm (half-pitch). The theoretically predicted resolution results from the convolution of the sample with the reference spot (see Eq. (1)). The shape and extent of the reference spot is a design parameter of the DOE. Our experimental reference spot is shown in Fig. 2. We measured a FWHM of approximately 180 nm (horizontal) and 160 nm (vertical) corresponding to a half pitch of 90 nm, 80 nm respectively (see supplement for details).

4. Discussion

Using a DOE for creating both the reference wave and the sample illumination, we achieved holographic reconstructions with a half-pitch resolution as low as 92 nm. Assuming the NA of the detector is matched, the resolution of our holography approach is mainly limited by the NA of the DOE. To achieve a larger NA of the DOE requires that the X-rays be diffracted to larger angles. An increase of the NA can be realized by either finer DOE structures or by using higher orders of diffraction. Currently, the limitation of electron beam based nano-lithography for the fabrication of the DOE is about 10 nm structure size. However, by generalizing our DOE generating algorithm to arbitrary diffraction orders, simulations showed that larger diffraction angles can be realized in high orders, at the (noncritical) cost of a reduced diffraction efficiency of the optics. Therefore, the minimum structure size which can be fabricated does not determine the resolution limit.

A comparison between the pinhole based and the DOE based holography approach shows that the pinhole based approach uses a significantly smaller part of incident X-rays (see Fig. 1). An estimation (for details see supplement) shows that for the presented experiment, the pinhole approach would use two order of magnitude less of the available photon flux. Therefore, the required exposure time for a similar signal-to-noise ratio of the hologram would have been

Optics EXPRESS

100-fold longer. As a result, the signal-to-noise ratio for single shot imaging is improved by one order of magnitude. In the classical pinhole holography setup, the scattered intensity decays rapidly from the central zero order beam with increasing spatial frequency. Therefore, the detector has to record typically a dynamic range of four orders of magnitude. Sine the DOE generates a hollow cone illumination, the zero order of the sample is distributed in a much wider ring-shaped area. As a consequence, the new holography setup works with conventional CCD-detectors with large pixel numbers and smaller dynamic range. Another advantage of the new approach is the fact that no pinhole is required in the sample plane, whereas the classical approach requires pinholes being located a few microns away from the sample. Therefore, in the DOE-based setup, the illuminating optics is decoupled from the sample plane giving more freedom for sample manipulation. For example, extended cryogenic biological samples could be investigated.

DOE based holography has a few natural extensions. Since holography is a full-field method, our proposed DOE-based holography method could be used for ultra-fast imaging with a setup that uses different optical path lengths similar to the femtosecond experiments described in [11,22]. However, the achievable lateral resolution has to be compromised with the temporal resolution. Since the hologram is essentially a far-field diffraction pattern, post-processing via ptychography methods can be applied. Such a ptychography step would enable increasing both the resolution and the accuracy of the recovered phase and amplitude. In serial femtosecond crystallography a large amount of samples are scanned and the diffraction patterns are then aligned and sorted before a real space reconstruction is performed (See for example [23] for identical samples.). Such methods could benefit from our DOE-based holography setup, which enables direct reconstruction of images of the samples. This reduces the computational cost of the alignment procedures and permits prescreening of the experimental data.

5. Conclusion

We described a new diffractive-optical-element-based holography setup and demonstrated experimentally the feasibility of the approach. An extended test sample was reconstructed with 92 nm resolution (half pitch). We showed that DOE-based holography overcomes some of the central limitations of previous X-ray Fourier-transform holography methods. The full potential of the new DOE based X-ray holography method can be employed at coherent free electron lasers or fourth generation ultimate storage ring sources with their highly coherent X-ray beams.

Funding. Seventh Framework Programme (grant agreement N°283570).

Acknowledgments. Measurements were carried out at the U41–SGM-TXM instrument at Helmholtz-Zentrum Berlin für Materialien und Energie. We thank the Helmholtz Zentrum Berlin for the allocation of synchrotron radiation beamtime.

Disclosures. "The authors declare no conflicts of interest."

Data availability. Data underlying the results presented in this paper are not publicly available at this time but may be obtained from the authors upon reasonable request.

Supplemental document. See Supplement 1 for supporting content.

References

1. A. Madsen, J. Hallmann, T. Roth, and G. Ansaldi, "Technical Design Report: Scientific Instrument MID," Tech. Rep. XFEL.EU TR-2013-005 (2013).
2. E. B. Malm, N. C. Monserud, C. G. Brown, P. W. Wachulak, H. Xu, G. Balakrishnan, W. Chao, E. Anderson, and M. C. Marconi, "Tabletop single-shot extreme ultraviolet fourier transform holography of an extended object," Opt. Express **21**(8), 9959–9966 (2013).
3. J. Geilhufe, B. Pfau, C. M. Günther, M. Schneider, and S. Eisebitt, "Achieving diffraction-limited resolution in soft-X-ray fourier-transform holography," Ultramicroscopy **214**, 113005 (2020).
4. T. Gorkhover, A. Ulmer, K. Ferguson, M. Bucher, F. R. N. C. Maia, J. Bielecki, T. Ekeberg, M. F. Hantke, B. J. Daurer, C. Nettelblad, J. Andreasson, A. Barty, P. Bruza, S. Carron, D. Hasse, J. Krzywinski, D. S. D. Larsson, A. Morgan, K. Mühlig, M. Müller, K. Okamoto, A. Pietrini, D. Rupp, M. Sauppe, G. van der Schot, M. Seibert, J. A. Sellberg, M. Svenda, M. Swiggers, N. Timneanu, D. Westphal, G. Williams, A. Zani, H. N. Chapman, G. Faigel, T.

Optics EXPRESS

Möller, J. Hajdu, and C. Bostedt, "Femtosecond X-ray fourier holography imaging of free-flying nanoparticles," Nat. Photonics **12**(3), 150–153 (2018).
5. G. Groh, *Holographie* (Verlag Berliner Union; Stuttgart, Berlin, Köln, Mainz: Kohlhammer, 1973).
6. B. Haas, J.-L. Rouvière, V. Boureau, R. Berthier, and D. Cooper, "Direct comparison of off-axis holography and differential phase contrast for the mapping of electric fields in semiconductors by transmission electron microscopy," Ultramicroscopy **198**, 58–72 (2019).
7. S. Eisebitt, J. Lüning, W. Schlotter, M. Lorgen, O. Hellwig, W. Eberhardt, and J. Stöhr, "Lensless imaging of magnetic nanostructures by X-ray spectro-holography," Nature **432**(7019), 885–888 (2004).
8. W. F. Schlotter, R. Rick, K. Chen, A. Scherz, J. Stöhr, J. Lüning, S. Eisebitt, C. Günther, W. Eberhardt, O. Hellwig, and I. McNulty, "Multiple reference Fourier transform holography with soft X-rays," Appl. Phys. Lett. **89**(16), 163112 (2006).
9. S. Marchesini, S. Boutet, A. E. Sakdinawat, M. J. Bogan, S. Bajt, A. Barty, H. N. Chapman, M. Frank, S. P. Hau-Riege, A. Szoeke, C. Cui, D. A. Shapiro, M. R. Howells, J. C. H. Spence, J. W. Shaevitz, J. Y. Lee, J. Hajdu, and M. M. Seibert, "Massively parallel X-ray holography," Nat. Photonics **2**(9), 560–563 (2008).
10. K. Nomura, N. Awaji, S. Doi, S. Isogami, K. Kodama, T. Nakamura, M. Suzuki, and M. Tsunoda, "Development of scanning type X-ray fourier transform holography," AIP Conf. Proc. **1365**, 277–280 (2011).
11. B. Pfau and S. Eisebitt, *X-ray Holography* (Springer International Publishing, Cham, 2016), pp. 1093–1133.
12. I. McNulty, J. Kirz, C. Jacobsen, E. H. Anderson, M. R. Howells, and D. P. Kern, "High-resolution imaging by fourier transform X-ray holography," Science **256**(5059), 1009–1012 (1992).
13. C. Pratsch, "New methods for high resolution 3d imaging with X-rays," Ph.D. thesis, Humboldt-Universität zu Berlin, Mathematisch-Naturwissenschaftliche Fakultät (2018).
14. S. Marchesini and A. Sakdinawat, "Shaping coherent X-rays with binary optics," Opt. Express **27**(2), 907–917 (2019).
15. K. Keskinbora, A. L. Levitan, and R. Comin, "Maskless fourier transform holography," Opt. Express **30**(1), 403–413 (2022).
16. H. Stiel, A. Blechschmidt, A. Dehlinger, R. Jung, E. Malm, B. Pfau, C. Pratsch, C. Seim, J. Tuemmler, and M. Zuerch, "2D and 3D Nanoscale Imaging Using High Repetition Rate Laboratory-Based Soft X-ray Sources," in *X-ray LASERS 2016*, vol. 202 *of Springer Proceedings in Physics* Kawachi, T and Bulanov, SV and Daido, H and Kato, Y, ed., Natl Inst Quantum & Radiol Sci & Technol, Kansai Photon Sci Inst (SPRINGER-VERLAG BERLIN, HEIDELBERGER PLATZ 3, D-14197 BERLIN, GERMANY, 2018), pp. 265–272. 15th International Conference on X-ray Lasers (ICXRL), Nara, JAPAN, MAY 22-27, 2016.
17. G. Schneider, P. Guttmann, S. Rehbein, S. Werner, and R. Follath, "Cryo X-ray microscope with flat sample geometry for correlative fluorescence and nanoscale tomographic imaging," J. Struct. Biol. **177**(2), 212–223 (2012).
18. F. Monroy, *Holography: Different Fields of Application* (IntechOpen, 2011).
19. MATLAB, *version 7.10.0 (R2010a)* (The MathWorks Inc., Natick, Massachusetts, 2010).
20. R. P. J. Nieuwenhuizen, K. A. Lidke, M. Bates, D. L. Puig, D. Gruenwald, S. Stallinga, and B. Rieger, "Measuring image resolution in optical nanoscopy," Nat. Methods **10**(6), 557–562 (2013).
21. C. A. Schneider, W. S. Rasband, and K. W. Eliceiri, "Nih image to imagej: 25 years of image analysis," Nat. Methods **9**(7), 671–675 (2012).
22. C. M. Guenther, B. Pfau, R. Mitzner, B. Siemer, S. Roling, H. Zacharias, O. Kutz, I. Rudolph, D. Schondelmaier, R. Treusch, and S. Eisebitt, "Sequential femtosecond X-ray imaging," Nat. Photonics **5**(2), 99–102 (2011).
23. J. Knoska, L. Adriano, S. Awel, K. R. Beyerlein, O. Yefanov, D. Oberthuer, G. E. P. Murillo, N. Roth, I. Sarrou, P. Villanueva-Perez, M. O. Wiedorn, F. Wilde, S. Bajt, H. N. Chapman, and M. Heymann, "Ultracompact 3D microfluidics for time-resolved structural biology," Nat. Commun. **11**(1), 657 (2020).